



## Vitamin B<sub>12</sub> effects on chlorinated methanes-degrading microcosms: Dual isotope and metabolically active microbial populations assessment



Diana Rodríguez-Fernández<sup>a,\*</sup>, Clara Torrentó<sup>b</sup>, Miriam Guivernau<sup>c</sup>, Marc Viñas<sup>c</sup>, Daniel Hunkeler<sup>b</sup>, Albert Soler<sup>a</sup>, Cristina Domènech<sup>a</sup>, Mònica Rosell<sup>a</sup>

<sup>a</sup> Grup de Mineralogia Aplicada i Geoquímica de Fluids, Departament de Mineralogia, Petrologia i Geologia Aplicada, Facultat de Ciències de la Terra, Universitat de Barcelona (UB), c/Martí Franquès s/n, 08028 Barcelona, Spain

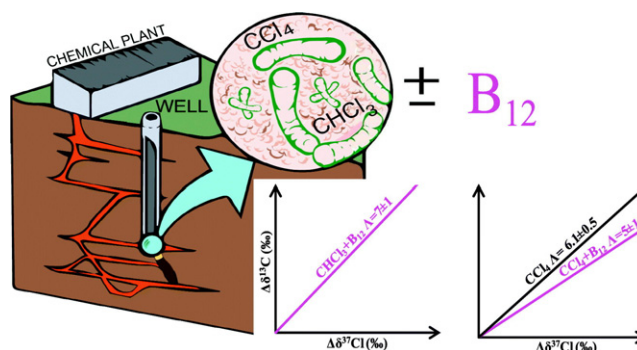
<sup>b</sup> Centre d'hydrogéologie et de géothermie, Université de Neuchâtel, Rue Emile-Argand 11, Neuchâtel 2000, Switzerland

<sup>c</sup> GIRO Joint Research Unit IRTA-UPC, IRTA, Torre Marimon, Caldes de Montbui E-08140, Spain

### HIGHLIGHTS

- B<sub>12</sub> catalyzed CT and CF anaerobic biodegradation in field-derived microcosms
- C-Cl CSIA and active microbial community used for CMs degradation assessment
- Distinct C-Cl isotope slope ( $\Lambda$ ) for B<sub>12</sub>-amended vs. unamended CT-treatments
- $\Lambda$  for CF biodegradation with B<sub>12</sub> similar to reported abiotic CF reduction by Fe(0)
- Higher activity of *P. stutzeri* and *Ancylobacter* in treatments with B<sub>12</sub>

### GRAPHICAL ABSTRACT



### ARTICLE INFO

#### Article history:

Received 27 June 2017

Received in revised form 21 September 2017

Accepted 8 October 2017

Available online 18 October 2017

Editor: D. Barcelo

#### Keywords:

Carbon tetrachloride

Chloroform

CSIA

Carbon chlorine isotope plot

MiSeq high-throughput sequencing

*Pseudomonas stutzeri*

### ABSTRACT

Field-derived anoxic microcosms were used to characterize chloroform (CF) and carbon tetrachloride (CT) natural attenuation to compare it with biostimulation scenarios in which vitamin B<sub>12</sub> was added (B<sub>12</sub>/pollutant ratio of 0.01 and 0.1) by means of by-products, carbon and chlorine compound-specific stable-isotope analysis, and the active microbial community through 16S rRNA MiSeq high-throughput sequencing. Autoclaved slurry controls discarded abiotic degradation processes. B<sub>12</sub> catalyzed CF and CT biodegradation without the accumulation of dichloromethane, carbon disulphide, or CF. The carbon isotopic fractionation value of CF ( $\epsilon_{C_{CF}}$ ) with B<sub>12</sub> was  $-14 \pm 4\%$ , and the value for chlorine ( $\epsilon_{Cl_{CF}}$ ) was  $-2.4 \pm 0.4\%$ . The carbon isotopic fractionation values of CT ( $\epsilon_{C_{CT}}$ ) were  $-16 \pm 6$  with B<sub>12</sub>, and  $-13 \pm 2\%$  without B<sub>12</sub>; and the chlorine isotopic fractionation values of CT ( $\epsilon_{Cl_{CT}}$ ) were  $-6 \pm 3$  and  $-4 \pm 2\%$ , respectively. *Acidovorax*, *Ancylobacter*, and *Pseudomonas* were the most metabolically active genera, whereas *Dehalobacter* and *Desulfitobacterium* were below 0.1% of relative abundance. The dual C-Cl element isotope slope ( $\Lambda = \Delta\delta^{13}C/\Delta\delta^{37}Cl$ ) for CF biodegradation (only detected with B<sub>12</sub>,  $7 \pm 1$ ) was similar to that reported for CF reduction by Fe(0) ( $8 \pm 2$ ). Several reductive pathways might be competing in the tested CT scenarios, as evidenced by the lack of CF accumulation when B<sub>12</sub> was added, which might be linked to a major activity of *Pseudomonas stutzeri*; by different chlorine apparent kinetic isotope effect values and  $\Lambda$  which was statistically different with and without B<sub>12</sub> ( $5 \pm 1$  vs  $6.1 \pm 0.5$ ), respectively. Thus, positive B<sub>12</sub> effects such as CT and CF degradation catalyst were quantified for the first time in isotopic terms, and confirmed with the major activity of species potentially capable of their degradation. Moreover, the indirect benefits

\* Corresponding author.

E-mail address: [diana.rodriguez@ub.edu](mailto:diana.rodriguez@ub.edu) (D. Rodríguez-Fernández).

of B<sub>12</sub> on the degradation of chlorinated ethenes were proved, creating a basis for remediation strategies in multi-contaminant polluted sites.

© 2017 Elsevier B.V. All rights reserved.

## 1. Introduction

The chlorinated methanes (CMs) carbon tetrachloride (CT) and chloroform (CF) are volatile organic compounds (VOCs) commonly found in groundwater. Although natural sources of CT and CF have been reported (Penny et al., 2010; Cappelletti et al., 2012), anthropogenic sources are more relevant given their use in many industrial activities (Doherty, 2000; Cappelletti et al., 2012). Both are considered possibly carcinogenic substances (Group 2B) by the International Agency for Research on Cancer and Disease Registry (2016).

There are no known organisms that metabolically degrade CT under neither oxic nor anoxic conditions (Penny et al., 2010). Under anoxic conditions, microbial CT degradation appears to be a non-specific co-metabolic reaction involving electron shuttles produced by facultative or strictly anaerobic bacteria and methanogenic Archaea (Penny et al., 2010). CT reduction is the predominant reaction mechanism which is either abiotically mediated by iron minerals and/or metals or biotically catalyzed (Lewis and Crawford, 1995). As seen in Scheme 1, in the CT reductive hydrogenolysis (pathway 1, Scheme 1), the first step involves an electron transfer leading to CF, while in other reduction processes two electrons are initially transferred, followed by hydrolytic substitution producing CO, formate, and CO<sub>2</sub> (hydrolytic reduction, pathway 2), or by thiolytic substitution leading to CS<sub>2</sub> (thiolytic reduction, pathway 3). Finally, CT reduction by the *Pseudomonas stutzeri* strain KC leads to CO<sub>2</sub> as the main product without CF formation, but with phosgene and thiophosgene as toxic intermediates (pathway 4).

CF biodegradation has been described under both oxic and anoxic conditions (Cappelletti et al., 2012). Under anoxic conditions, the following pathways are reported in the literature: CF dehalorespiration and co-metabolic reductive dechlorination to DCM (pathway 1, Scheme 1), CF reductive elimination to CH<sub>4</sub> (pathway 1a), and a first reduction followed by hydrolysis and final oxidation to CO and CO<sub>2</sub> (pathway 2). The mentioned anaerobic CF pathways were also described abiotically (He et al., 2015).

Redox active corrinoids such as vitamin B<sub>12</sub>, a cofactor for some dehalogenase enzymes (Banerjee and Ragsdale, 2003), catalyze the reductive biodegradation of CT to CO, CO<sub>2</sub>, or CS<sub>2</sub>, which suggests degradation through pathways 2 and 3 (Scheme 1), whereas toxic CF (through pathway 1, Scheme 1) becomes a minor product, possibly

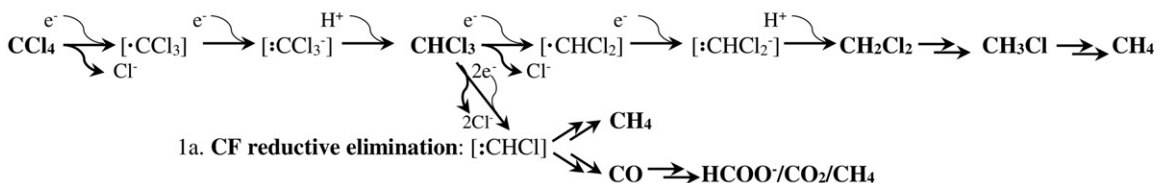
because B<sub>12</sub> stimulates further CF degradation (via pathway 1a or 2) (Cappelletti et al., 2012). However, it is unknown in which proportion these CMs degradation pathways take place in complex mixed cultures, and if they happen biotic or abiotically depending on the media composition. It is also unknown how different B<sub>12</sub>/pollutant ratios impact this pathway selection, because the available data to date is only in terms of consumption rates or the characterization of by-products (Becker and Freedman, 1994; Hashsham et al., 1995; Workman et al., 1997; Zou et al., 2000; Guerrero-Barajas and Field, 2005a, 2005b; Shan et al., 2010). Hence, isotope and microbiological tools are proposed hereafter to better assess the natural attenuation and changes of CMs caused by B<sub>12</sub> in field-derived anoxic microcosms.

Compound specific isotope analysis (CSIA) allows one to confirm degradation when monitoring of the concentration of parental or by-products is not conclusive (Elsner, 2010). The calculation of the extent of isotopic fractionation ( $\epsilon$ ) in the laboratory follows a Rayleigh approach (Elsner et al., 2005) through Eq. (1) in which  $\delta_0$  and  $\delta_t$  are the isotope values (in per mil units, ‰, relative to international standards) of C or Cl at the initial start and after a given time (t) respectively, and f is the fraction of substrate remaining at time t. This calculation affords knowledge about whether degradation will be qualitatively detected in the studied field, and provides information about the reaction mechanism which is occurring by comparing the apparent kinetic isotope effects (AKIEs) to those reported in the literature and to the theoretical kinetic isotope effects (KIEs) (Elsner et al., 2005).

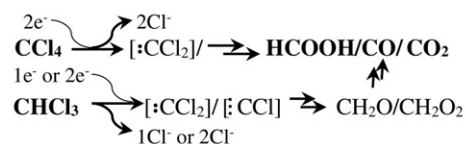
$$\ln \frac{\delta_t + 1000}{\delta_0 + 1000} = \frac{\epsilon}{1000} \ln f \quad (1)$$

This approach however, has some limitations, since different AKIEs values for reactions undergoing the same bond cleavage can be obtained due to masking by rate limiting steps, or by secondary or superimposed isotope effects (Nijenhuis and Richnow, 2016). Thus, dual element isotope plots (2D-CSIA) allow a better distinction within different reactions, since slopes (e.g.  $\Lambda = \Delta\delta^{13}\text{C}/\Delta\delta^{37}\text{Cl}$ ) are expected to be reaction-specific (Cretnik et al., 2013) and non-masked because both elements are affected to the same extent (Elsner et al., 2005). To our knowledge, only one study has explored  $\Lambda$  values for abiotic CF engineered transformation reactions (Torrentó et al., 2017), and no  $\Lambda$

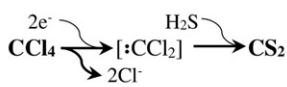
### 1. CT or CF hydrogenolysis



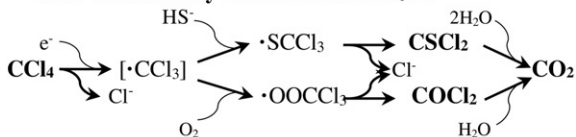
### 2. CT or CF hydrolytic reduction



### 3. CT thiolytic reduction



### 4. CT reduction by *Pseudomonas stutzeri*



**Scheme 1.** Hypothetical CT (carbon tetrachloride) and CF (chloroform) reductive pathways according to Lewis and Crawford (1995), Field and Sierra-Alvarez (2004), Song and Carraway (2006), Penny et al. (2010), Cappelletti et al. (2012), and Torrentó et al. (2017).

values for biotic CF, or for abiotic or biotic CT degradation reaction models exist yet. Due to the limited  $\Lambda$  values of reference reactions, linking AKIE and  $\Lambda$  information with the activity of potential CT and CF microbial degraders can be worthwhile to gain insights into the natural attenuation and changes of CMs on the microbial population produced during bioremediation. RNA-based analyses provide more insight into active biologic processes than physiologic or genetic capability alone (Yargicoglu and Reddy, 2015). Next-Generation Sequencing (NGS) technologies, such as Miseq, have prompted a shift towards high-throughput methods for characterizing both total and metabolically active (16S rRNA from active ribosomes and total RNA, analyzed from synthesized cDNA) microbial communities (Pelissari et al., 2017).

The main aim of the present study was to characterize the anaerobic CT and CF biodegradation potential of indigenous microbiota from the monitored contaminated Òdena site (Barcelona, Spain) (Palau et al., 2014; Torrentó et al., 2014), and also to characterize the effects of vitamin B<sub>12</sub>, as a bioremediation strategy, on the microbial community and on degradation pathways, for further field applications. B<sub>12</sub> amended and unamended microcosm batch experiments were used for (1) monitoring the concentration of parental and by-product compounds and  $\delta^{13}\text{C}$  and  $\delta^{37}\text{Cl}$  to evidence degradation; (2) characterizing the active microbial community by RNA-based NGS to assess the effect of B<sub>12</sub> addition on the microbial populations; and (3) determining the  $\epsilon\text{C}$ ,  $\epsilon\text{Cl}$ , the corresponding AKIEs and  $\Lambda$  of each compound and treatment to study the degradation pathways.

## 2. Material and methods

### 2.1. Experimental set-up

Following the Fennell et al. (2001) procedure, preliminary microcosm assays were performed with homogeneous slurry (groundwater and sediments) collected in June 2012 from the bottom portion (17 m.b.g.s.) of an iron-reducing well at the Òdena site (Palau et al., 2014). The original amounts of the pollutants present in the field (chlorinated methanes, ethenes and ethanes, BTEXs, and traces of pesticides (Torrentó et al., 2014)) remained unchanged in these preliminary microcosm assays. These preliminary microcosm assays served to prove the natural attenuation of CMs, which was accelerated with the addition of 10  $\mu\text{M}$  of B<sub>12</sub> (data not shown).

For studying the effect of different amounts of B<sub>12</sub> on the degradation of CMs in detail, a new slurry was collected from the same well in February 2014. The slurry was flushed with N<sub>2</sub>(g) during two hours inside an anoxic N<sub>2</sub>(g)-filled glovebox to remove the large original concentrations of VOCs and to add known amounts of CF and CT. According to Guerrero-Barajas and Field (2005a, 2005b), three scenarios exist for each target compound: (i) without the addition of vitamin B<sub>12</sub>, called “pollutant without B<sub>12</sub> treatment” abbreviated as CFw/oB or CTw/oB; (ii) with a molar ratio of vitamin B<sub>12</sub>/pollutant of 0.01, called “0.01B/pollutant treatment”; and (iii) with a molar ratio of 0.1, called “0.1B/pollutant treatment”; the pollutant being CT (99% Panreac) or CF (99% Merck) depending on the case. Live treatments were run in quintuplicate using 120 mL-serum bottles filled with 100 mL of slurry, which were inoculated with a theoretical pollutant concentration of 200  $\mu\text{M}$ , referred to as the liquid volume, and with the corresponding B<sub>12</sub> volume (0, 2, or 20  $\mu\text{L}$ ). The bottles were filled-up inside an anoxic glove box and sealed with grey PTFE stoppers. Parallel series with triplicate heat-killed (KI) controls were performed to discard abiotic processes. KI controls were filled with 100 mL of slurry and sealed inside the glovebox prior to autoclaving in three cycles of 20 min at 121 °C. The same amounts of pollutant and B<sub>12</sub> in comparison to the equivalent live treatment were subsequently added by using N<sub>2</sub>-purged sterile syringes. KI controls were started 43 h after the live samples. Static incubation in darkness at room temperature was performed for all treatments during the 376 days long experimental period (t<sub>10</sub>).

### 2.2. Sampling

Samples for chemical and isotopic analyses were periodically taken using sterilized syringes and filtered through 0.2  $\mu\text{m}$ -nylon sterilized filters (Millipore) from three of the replicate bottles and kept refrigerated at 4 °C in 2.5 mL crimped vials. A sample from the flushed slurry without amendments was taken for VOCs concentration analysis and DNA was extracted for studying the total bacterial population present at the initial time (t<sub>0</sub>) by DGGE and 16S rRNA MiSeq high-throughput sequencing. In addition, when the degradation of significant target contaminants was detected (at 85 days, t<sub>3</sub>, from all B<sub>12</sub> amended bottles, and at t<sub>10</sub> from all live treatments), samples were taken from one of the two untouched replicates for total RNA extraction (then retrotranscribed to cDNA) for further DGGE and 16S rRNA MiSeq high-throughput sequencing. The concentrations of VOCs,  $\delta^{13}\text{C}_{\text{CT}}$ , and  $\delta^{13}\text{C}_{\text{CF}}$  were also measured in these replicates just before the extraction (M\_S bottles in the figures).

### 2.3. Chemical analyses

Due to volume limitations, the concentration of VOCs and C and Cl isotope analyses of CT and CF were prioritized. The concentration of VOCs was measured in the *Centres Científics i Tecnològics de la Universitat de Barcelona* (CCiT-UB) by headspace (HS)-gas chromatography (GC) - mass spectrometry (MS) as explained in Torrentó et al. (2014). The error based on replicate measurements was below 10% for all compounds.

To compare the concentration decrease kinetics among the treatments and the literature, aqueous concentration data of CT and/or CF versus time was fitted to a pseudo-first-order rate model according to Eq. (2), where C is the target chlorinated compound concentration in  $\mu\text{M}$ , t is the time in days, and k' is the pseudo-first-order rate constant (days<sup>-1</sup>), assuming that all the removal of CT and CF was due to a degradation process.

$$dC/dt = -k'C \quad (2)$$

The k' was obtained using the integrated form of Eq. (2), shown in Eq. (3) where C<sub>0</sub> is the initial concentration of the chlorinated compound ( $\mu\text{mol/L}$ ).

$$\ln f = \ln C/C_0 = k't \quad (3)$$

Uncertainty was obtained from 95% confidence intervals (CI).

Temperature, pH, and anions and cation concentrations were measured when possible (see SI for further details).

### 2.4. Isotope analyses

Due to volume limitations,  $\delta^{13}\text{C}$  and  $\delta^{37}\text{Cl}$  were measured in different replicates of the same treatment and incubation time.  $\delta^{13}\text{C}$  analyses were performed in CCiT-UB by HS - solid-phase micro-extraction (SPME)-GC-isotope ratio MS (IRMS), as explained in Martín-González et al. (2015). According to the standard deviation of the daily standards of each compound (SD  $\leq 0.5$ , n = 24), a total instrumental uncertainty (2 $\sigma$ ) of  $\pm 0.5\text{‰}$  was considered (Sherwood Lollar et al., 2007), given that volume limitation prevented duplication of the measurements.  $\delta^{37}\text{Cl}$  analyses were performed in the University of Neuchâtel using a HS-GC-quadrupole MS (qMS), as explained in Heckel et al. (2017). Each  $\delta^{37}\text{Cl}$  value and its analytical uncertainty (2 $\sigma$ , in all cases below  $\pm 0.5\text{‰}$ ) were determined on the basis of ten injections, and the working standards were interspersed along the sequence.

Isotopic mass balances were calculated following Eq. (4), where x is the molar fraction of each compound relative to the total molar mass of CMs from which isotopic values are available at each time. The equation assumes only the hydrogenolysis pathway with the available isotopic

data from CMs, since potential gas products (CH<sub>4</sub>, CO, CO<sub>2</sub>, formate, phosgene, and thiophosgene) were not measured.

$$\delta^{13}\text{C}_{\text{SUM}}(\text{‰}) = x_{\text{CT}}\delta^{13}\text{C}_{\text{CT}} + x_{\text{CF}}\delta^{13}\text{C}_{\text{CF}} + x_{\text{DCM}}\delta^{13}\text{C}_{\text{DCM}} \quad (4)$$

For AKIE calculations, carbon and chloride  $\epsilon$  values determined by the Rayleigh approach (Eq. (1)) were used according to Eq. (5), where  $n$  is the total number of the atoms of the considered element (E) in the target molecule,  $x$  the number of atoms located at the reactive site, and  $z$  the number of atoms in intramolecular isotopic competition.

$$\text{AKIE}_E \approx \frac{1}{1 + \left(\frac{n \times z}{x} \times \frac{\epsilon}{1000}\right)} \quad (5)$$

AKIE<sub>C</sub> was calculated using  $n = x = z = 1$  for both compounds, while AKIE<sub>Cl</sub> was calculated using  $n = x = z = 4$  for CT and  $n = x = z = 3$ , for CF.

## 2.5. Microbial community abundance and diversity analyses

### 2.5.1. DNA-based study at the initial time

To have a sample representative of the initial time ( $t_0$ ), a slurry was sampled after flushing and before the addition of target compounds and B<sub>12</sub>. This sample was used for studying the total bacterial population through DNA extraction by following the same procedure detailed in the subsequent sections for RNA.

### 2.5.2. Total genomic DNA and RNA extraction

15 mL of slurry from microcosms at different incubation times were collected in triplicate and centrifuged at 4000 g/30' and 4 °C. The supernatants were removed and the pellets were stored immediately at –80 °C until further analysis. Total RNA and DNA were extracted in triplicate from known weights of each sample with the PowerMicrobiome™ RNA Isolation Kit, Catalog #26000-50 (MoBio Laboratories Inc., Carlsbad, CA, USA), according to the manufacturer's instructions. Purified total RNA was obtained by the removal of the co-extracted DNA with DNase I (provided by the kit) at 25 °C for 10 min, and the subsequent inactivation of DNase I with EDTA 50 mM (Thermo Scientific Fermentas, USA) at 75 °C for 5 min. Reverse transcription polymerase chain reaction (RT-PCR) for cDNA synthesis from the obtained mRNA was performed using the PrimeScript™ RT Reagent Kit (Takara Bio Inc., Japan). The reaction was carried out in a volume of 30 µL, which contained 15 µL of purified mRNA, 6 µL of PrimeScript™ buffer, 1.5 µL of the enzyme mix, 1.5 µL of Random 6 mers, and 6 µL of RNase Free dH<sub>2</sub>O.

### 2.5.3. DGGE analyses

Three primer sets selectively amplified bacterial (F341GC/R907) and archaeal (ArchF0025/ArchR1517; nested ArchF344/ArchR915GC) 16S rRNA gene fragments. The PCR amplification of the hypervariable V3-V5 region from the 16S rRNA gene of both domains, and the DGGE profiles and sequencing were performed as previously reported by Palatsi et al. (2010). The sequences were chimera-checked by using the Bellerephon on-line tool (DeSantis et al., 2006), and aligned against the GenBank database by using the BLASTn and RDP alignment tool comparison software. The sequences were submitted to Genbank (NCBI) with the accession numbers (KY921708–KY921709).

### 2.5.4. *cfrA* gene expression

In order to detect the presence and activity of *Dehalobacter* sp., *cfrA* encoding gene of the CF reductive dehalogenase alpha subunit (Chan et al., 2012; Tang and Edwards, 2013) was assessed by the qPCR technique as described in Tang and Edwards (2013). For the standard curve, it was designed a synthetic gene by using gBlocks® Gene Fragments (IDT, Integrated DNA Technologies). The *cfrA* sequence belongs to *Dehalobacter* sp. enrichment culture clone rdhA01 (GenBank

sequence database: JX282329.1). Ten-fold serial dilutions from synthetic genes were subjected to qPCR assays in duplicate showing a linear range between 10<sup>1</sup> and 10<sup>8</sup> gene copy numbers per reaction to generate standard curves. qPCR reactions fitted quality standards: efficiencies were between 90 and 110% and R<sup>2</sup> above 0.985. All results were processed by MxPro™ QPCR Software (Stratagene, La Jolla, CA) and were treated statistically.

### 2.5.5. 16S rRNA Illumina-sequencing of the active microbial populations

A deep microbial diversity assessment of the metabolically active populations was performed by means of 16S rRNA (RNA-based) Illumina (MiSeq) high-throughput sequencing, targeting the bacterial 16S rRNA V1-V3 region, by utilizing the Illumina MiSeq sequencing platform. The obtained DNA reads were compiled in FASTq files for further bioinformatic processing. Trimming of the 16S rRNA barcoded sequences into libraries was carried out using QIIME software version 1.8.0 (Caporaso et al., 2010a). Quality filtering of the reads was performed at Q25, prior to the grouping into Operational Taxonomic Units (OTUs) at a 97% sequence homology cutoff. The following steps were performed using QIIME: Denoising using Denoiser (Reeder and Knight, 2010); reference sequences for each OTU (OTU picking up) were obtained via the first method of the UCLUST algorithm (Edgar, 2010); for sequence alignment and chimera detection the algorithms PyNAST (Caporaso et al., 2010b) and ChimeraSlayer (Haas et al., 2011) were used. OTUs were then taxonomically classified using RDP Naïve Bayesian Classifier (2.2) with a bootstrap cutoff value of 80%, and compiled to each taxonomic level (Wang et al., 2007). To evaluate the alpha diversity of the samples, the number of OTUs, the inverted Simpson index, Shannon index, Goods coverage, and Chao1 richness estimators were calculated using the Mothur software v.1.35.9 (<http://www.mothur.org>) (Schloss et al., 2009). All the alpha-diversity estimators were normalized to 70,000 (the lower number of contigs among the different samples). Data from the MiSeq NGS assessment were submitted to the Sequence Read Archive (SRA) of the National Center for Biotechnology Information (NCBI) under the study accession number SRP090228.

## 3. Results and discussion

### 3.1. Biodegradation evidence

The elimination of VOCs by N<sub>2</sub> flushing of the slurry was not complete, as CT was much more efficiently flushed than CF (Table 1), although the remaining CF represented around a 10–20% of the total initial CF concentration in the CF treatments. The measured initial CT concentrations (Table 1) were four times smaller than the expected, likely due to the sorption of the slurry, while CF agreed better with the expected values, consistent with its lower tendency to sorb (Cappelletti et al., 2012).

**Table 1**

The average concentrations of VOCs ( $n$  measurements specified in parentheses) for the initial slurry after N<sub>2</sub> flushing ( $t_0$ ) and live and heat-killed controls for all treatments of each parental compound (including together with and without B<sub>12</sub>) in the first sampling (live treatments: 90 min after starting; heat-killed controls: 60 min after starting) expressed as µM at the liquid phase of the experimental bottle.

	Slurry $t_0$	CT treatments		CF treatments	
		Live	Heat-killed	Live	Heat-killed
CT	2	40 ± 17 (12)	26 ± 10 (15)	8 ± 5 (8)	4.5 ± 0.4 (9)
CF	26	<2	<2	132 ± 10 (9)	189 ± 37 (9)
DCM	0.4	<4	<4	<4	<4
CS <sub>2</sub>	0.7	<0.7	<0.7	<0.7	<0.7
PCE	0.4	<2	<2	<2	<2
TCE	5	<2	<2	<2	<2
cDCE	9	2 ± 2 (8)	1.4 ± 0.1 (9)	10.0 ± 0.8 (3)	3.2 ± 0.2 (3)

Fluctuations in CF and CT concentration were observed in all the KI controls (Fig. 1), but they were not accompanied by an increase in the concentration of the expected metabolites neither by shifts in carbon nor in chlorine isotopic signatures ( $\delta^{13}\text{C}_{\text{CF}} = -41.7 \pm 0.3\%$ ,  $n = 9$ ;  $\delta^{37}\text{Cl}_{\text{CF}} = -2.6 \pm 0.1\%$ ,  $n = 3$ ;  $\delta^{13}\text{C}_{\text{CT}} = -40.4 \pm 0.8\%$ ,  $n = 19$ ;  $\delta^{37}\text{Cl}_{\text{CT}} = -0.8 \pm 0.1\%$ ,  $n = 4$ ) (Fig. 2). This would suggest that degradation is not occurring. The observed fluctuations in concentration could be due to sorption-desorption processes (Riley et al., 2010). This lack of CF degradation in the KI controls was consistent with results obtained in heat-killed controls amended with cobalamins performed by Guerrero-Barajas and Field (2005a), but not in the case of CT KI controls conducted by Guerrero-Barajas and Field (2005b). Guerrero-Barajas and Field (2005b) and Egli et al. (1990) pointed to CT and CF degradation by heat-killed cells, leading to DCM or  $\text{CO}_2$ , but at a markedly reduced rate compared to live treatments. The absence of CT degradation in our KI controls is also contrary to other studies (Hashsham et al., 1995; Puigserver et al., 2016). These degradation differences could be partially attributed to different slurry compositions, which may differ in the potential presence of reducing agents, such as sulfide or iron minerals, capable of supplying electrons for the abiotic reduction of CMs, which were not measured in any case.

The CT and CF concentration behaviour in triplicates of the same treatment were quite reproducible over time (Fig. A1), which permitted  $\delta^{13}\text{C}$  and  $\delta^{37}\text{Cl}$  analyses in different replicates. CF biodegradation only occurred in the presence of  $\text{B}_{12}$ . In the CFw/oB treatment, the CF concentration fluctuated (Fig. 1A), but  $\delta^{13}\text{C}_{\text{CF}}$  did not vary significantly ( $-40.8 \pm 0.8\%$ ,  $n = 7$ ) (Fig. 2A). On the other hand, in the presence of  $\text{B}_{12}$  in the 0.01B/CF treatment, a CF concentration decrease (Fig. 1B) was accompanied by significant enrichment of the heavy isotopes for both C and Cl ( $\Delta\delta$ , 23 and 3‰, respectively, at  $t_{10}$ ), indicative of normal isotope effects (Fig. 2A, B). In the 0.1B/CF treatment, CF was completely consumed before 72 days (Fig. 1C) which did not allow isotope measurements in the samples. No  $\text{CS}_2$  accumulation (Fig. A2) was detected in any CF treatment, and significant transient DCM accumulation only occurred for the 0.01B/CF treatment after around 200 days (Fig. A3B).

CT degradation occurred both without and with  $\text{B}_{12}$ , being accelerated in the latter. The decrease of the CT concentration in the CTw/oB treatment (Fig. 1D) was accompanied by significant  $\Delta\delta^{13}\text{C}$  and  $\Delta\delta^{37}\text{Cl}$  (up to 32‰ and 6‰, at  $t_{10}$ , respectively, Fig. 2C), indicating natural biodegradation. CTw/oB treatments showed a change in the CT isotope enrichment trend after 211 days (Fig. 2C, D), a change that was also observed in the CT degradation rates (Fig. A4). CF was yielded as a by-product in the CTw/oB treatment, and its concentration increased over time (Fig. 1D). The  $\delta^{13}\text{C}_{\text{CF}}$  depletion pattern during the first 200 days was probably due to the combined effect of both the produced and background CF isotopic signature (Fig. 2E, F). In addition, the least CF isotopic fractionation observed (Fig. 2E, F) could be explained by isotopically-sensitive branching (Zwank et al., 2005): CF might be formed in parallel with other non-analyzed products (as evidenced by non-closed isotopic mass balance, data not shown), and the enrichment effect of further CF degradation was discarded without  $\text{B}_{12}$ .

Complete CT consumption was observed in the 0.01B/CT and 0.1B/CT treatments after 110 and 72 days, respectively (Fig. 1E–F). Both treatments showed significant and similar carbon and chlorine isotopic enrichment trends (Fig. 2C, D). In the 0.01B/CT treatment, the CF concentration increased over time as a by-product (Fig. 1E), whereas in the 0.1B/CT treatment, a decrease in the CF concentration was detected (Fig. 1F). CF (hypothetical yield  $\pm$  background) underwent isotopic enrichment, which was more significant once parental CT was totally consumed (Fig. 2C–F). This suggested that the 0.1B/CT ratio could be an eligible proportion to degrade both the parental CT and their degradation by-product (CF), if applied in the field site at the studied well. There was an absence of significant DCM or  $\text{CS}_2$  accumulation in all the CT treatments (Fig. A2, A3).

Pseudo-first rate constant values of concentration removal kinetics ( $k'$ , Fig. A4) confirmed the catalytic effect of  $\text{B}_{12}$  (e.g.  $k' = 0.003 \pm 0.001 \text{ d}^{-1}$  for 0.01B/CF and  $k' = 0.08 \pm 0.06 \text{ d}^{-1}$  for 0.1B/CF). These values cannot be directly compared to those reported in similar microcosm studies (Guerrero-Barajas and Field, 2005a, 2005b), since they

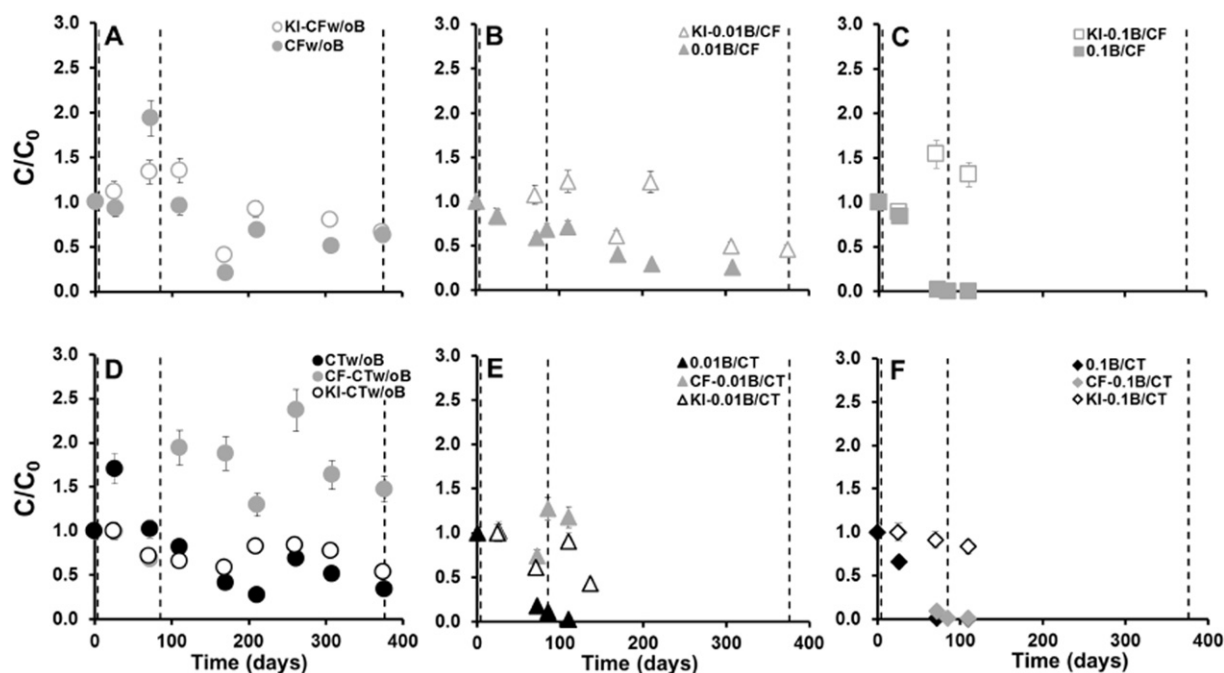


**Fig. 1.** Evolution of CF (grey) and CT (black) concentration (in  $C/C_0$ ) in replicate 1 (from which C-CSIA measurements were done) of the CF (upper panels) and CT (lower panels) treatments: CFw/oB (A), 0.01B/CF (B), 0.1B/CF (C), CTw/oB (D), 0.01B/CT (E), and 0.1B/CT (F).  $C/C_0$  were calculated from the total  $\mu\text{mol}$  in the bottle taking into account Henry's law constant at 24 °C according to Staudinger and Roberts (2001). CF evolution, as a potential product in the CT treatments, is also shown in D, E, and F. The evolution of parental compounds in replicate 1 from the corresponding heat-killed control (KI) experiments are shown for each treatment (empty symbols). No significant changes in the background CF were detected in CT-KI along the incubation time (data not shown). Dashed lines show the sampling times of the microbial analyses ( $t_0$ ,  $t_3$ , and  $t_{10}$ ). The error bars show the uncertainty in the concentration measurements. When not visible, error bars are smaller than the symbols.

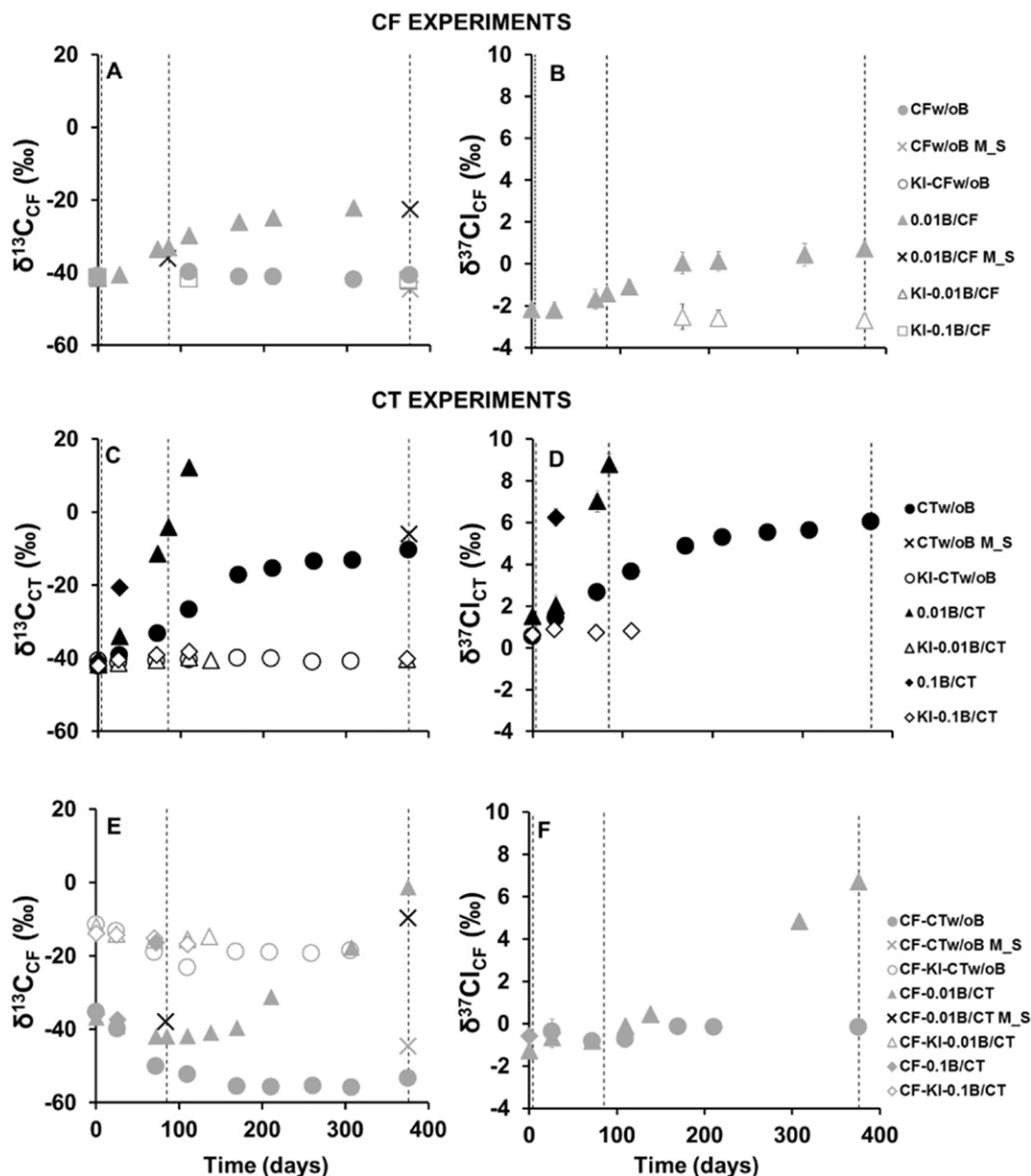


**Fig. 2.** The evolution of the CF and CT carbon (left panels), and chlorine (right panels) isotope composition (‰) over time, measured in replicates 1 and 2, respectively, of each treatment with CF (A, B) and CT (C, D) as target compounds, and CF (E, F) as a CT by-product. CF concentrations in the 0.1B/CF treatment decreased rapidly, and were therefore too low for isotopic measurements (no data points). The cross shaped symbol corresponds to carbon isotope data of the replicates (M\_S bottles) used for microbial sampling (indicated in dashed lines). CT in 0.01B/CT and CT and CF, as a by-product, in the 0.1B/CT treatments were below the detection limit for carbon isotopic measurements (no data points) in replicates for microbial sampling. When not visible, error bars are smaller than the symbols.

were performed at different temperatures and with a different sludge composition. However, the ratios obtained for CT ( $k'_{0.1\text{B}/\text{CT}}$  to  $k'_{\text{CTw/oB}}$ ) were indeed similar (6 to 12) to Guerrero-Barajas and Field (2005b) (see Table A1). The  $k'$  for the CTw/oB treatment changed from  $0.010 \pm 0.003 \text{ d}^{-1}$  towards a value of  $0.005 \pm 0.002 \text{ d}^{-1}$  after 211 days. This half reduction of the kinetics might be due to CT inhibition by CF yield, redox mediators, and/or the consumption of other required nutrients (Chan et al., 2012; Lima and Sleep, 2010).

Low DCM amounts prevented the obtaining of its isotopic composition, and isotopic mass balances calculated with CF and CT did not close in those treatments where degradation was proved (all except the KI controls and CFw/oB), with a maximum difference,  $\Delta(\delta_{\text{sum}} - \delta_{\text{initial}})$ , of 40‰ in the case of the 0.1B/CT treatment. This is evidence of the degradation of further products or/and the existence of parallel pathways producing non-analyzed gas products ( $\text{CH}_4$ , CO,  $\text{CO}_2$ , formate, phosgene, and tiophosgene).

$\Delta\delta^{13}\text{C}$  of the background PCE and cDCE was detected in the 0.1B/pollutant experiments (up to 11.6 and 5.3‰, respectively), when the CT and CF concentrations decreased to levels under the detection limit, while  $\delta^{13}\text{C}_{\text{PCE}}$  remained constant ( $-26.6 \pm 0.1\%$ ), if CF was still in solution in the 0.1B/CF treatment (Fig. 3). These inhibition effects of CMs on the degradation of chlorinated ethenes were previously reported in the literature (Bagley et al., 2000; Duhamel et al., 2002; Futagami et al., 2006), but never proved by isotopic data.

### 3.2. Active microbial populations assessment

Samples for DGGE and NGS analyses taken at  $t_0$ ,  $t_3$ , and  $t_{10}$  were representative of different degradation stages in each treatment (detailed in 'Microbial assessment' section, SI). The results of NGS revealed a metabolically active microbial diversity greater than that observed for DGGE (Fig. A5, Table A2), and allowed the identification of active species

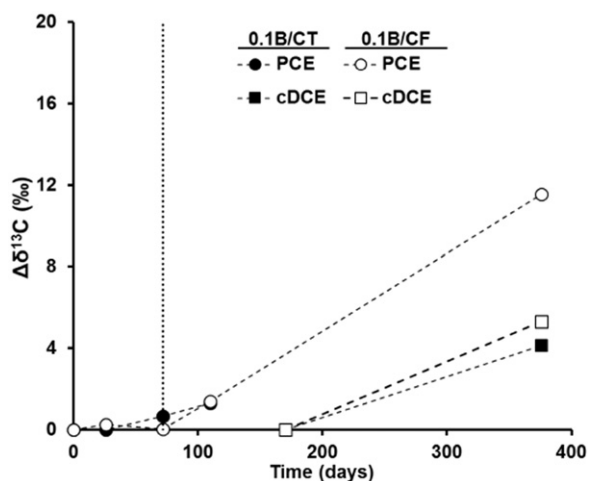


**Fig. 3.** PCE and cDCE carbon isotope composition variation (‰) over time in the 0.1B/CT and 0.1B/CF treatments. The vertical line shows the time when the concentrations of target compounds (CT and CF) in both treatments decreased below the detection limit.

within the autochthonous community (Table 2). Well-known organohalide-respiring bacteria (OHRB) according to Adrian and Löffler, 2016 such as *Dehalococcoides*, *Sulfurospirillum*, *Geobacter*, *Desulfosporosinus*, *Dehalobacter*, and *Desulfitobacterium* spp. (the last two with known CF reductive dehalogenases, Tang and Edwards, 2013; Ding et al., 2014), were not metabolically active (<0.1% relative abundance, RA) at any of the sampled times, and were not present at the initial time using DNA-based analyses (Table 2). In addition, the dehalogenase encoding *cfra* gene was below the detection limit (<10<sup>2</sup> *cfra* copies mL<sup>-1</sup>, data not shown) in all t<sub>3</sub> samples, confirming the low metabolic activity of *Dehalobacter* spp. at this time. The low or non-existent presence and activity of OHRB could be connected with the well-known antagonistic effects of co-contaminants such as CMs against these TCE/PCE degrading bacteria (Futagami et al., 2006; Cappelletti et al., 2012; Tang et al., 2016); with the reported CT

inhibition of CF respiration by *Dehalobacter* (Lee et al., 2015), or with the competition with other active microbial populations from the phylum Proteobacteria (mentioned below), which would require further investigation.

In all treatments, the greatest represented phylum was Proteobacteria (RA > 80%) (Table 2, Fig. A6), and this phylum is described in better detail hereafter. In the CTw/oB treatment at t<sub>10</sub>, the predominantly active genus was the facultatively anaerobic *Acidovorax* (53%) (Table 2, Fig. A7, Table A3), being more abundant than in the CT treatments with B<sub>12</sub> (23 to 27%). *Acidovorax* sp. 2AN has been described as capable of anoxic Fe(II)-oxidation-enhanced chemotrophic growth coupled to NO<sub>3</sub><sup>-</sup> reduction (Chakraborty et al., 2011), and an average NO<sub>3</sub><sup>-</sup> concentration of 40 ± 12 μM (n = 16) (Table A6) in the parental CT treatments would support its growth. Lima and Sleep (2010) reported inhibition of the microbial activity related to CT degradation by 0.2–0.4 μM of CF. The authors observed a decrease in the number of bacterial species, including *Acidovorax*, under iron-limiting conditions. In the present study, the initial CF concentrations (Table 1) were close to those considered inhibitory in the reported study by Lima and Sleep (2010), which supports that the lowering of δ<sup>13</sup>C<sub>CT</sub> enrichment after 211 days in the CTw/oB treatment (Fig. 2C, D) might be due to the toxic effects of CF accumulation (Fig. 1D) on CT dechlorinating microorganisms. This might proceed through a general inhibition of the metabolic processes (Cappelletti et al., 2012) rather than by enzyme competition. Since bacterial community diversity was examined only at time t<sub>0</sub> and time t<sub>10</sub> (after 376 days), this hypothesis cannot be confirmed in terms of changes in the bacterial population.

The genus *Pseudomonas* presented two predominantly active OTUs in all analyzed samples, belonging to *Pseudomonas lingynensis* (6–57% RA, similarity of 99.6%) and *Pseudomonas stutzeri* (1–10% RA, similarity of 99–100%) (Table A4). *P. stutzeri* constituted 9–10% RA (Table 2) in the B<sub>12</sub>-amended CT treatments at t<sub>3</sub>, whereas it represented only around 1% RA in the CTw/oB treatment at t<sub>10</sub>, suggesting a relationship between this species and B<sub>12</sub>. The *P. stutzeri* strain KC is able to denitrify and to co-metabolically transform CT to CO<sub>2</sub> and non-volatile products (pathway 4, Scheme 1) by excreting a siderophore related to Fe chelation, enabling extracellular CT dehalogenation. Since

**Table 2**

Biodiversity of bacterial populations expressed as the relative abundance (RA, in %) at the Phylum/Family/Genus level according to the RDP Bayesian Classifier database (at the genus level with a bootstrap confidence above 80%), obtained from the M\_S bottles. The most abundant phyla (above 1% of the RA in at least one sample) as well as striking genera and/or species are shown. Detailed abundances for all the detected genera are shown in the SI (Table A4). The remainder of the phyla up to 100% are included in "Others". The initial sample (t<sub>0</sub>\_DNA) was direct 16S rRNA (DNA-based) analysis of the flushed slurry without amendments, while the remaining samples are 16S rRNA (RNA-based) extracted from the different CF and CT selected treatments and sampling points (t). Diversity, richness, and coverage indexes are shown in Table A5.

Phylum	Family	Genus/species	DNA t <sub>0</sub>	CTw/oB t <sub>10</sub>	0.1B/CT t <sub>3</sub>	0.1B/CT t <sub>3</sub>	0.1B/CF t <sub>3</sub>
Total contigs 478,204)			70,705	113,413	98,700	88,726	106,660
Total OTUs (1087)			843	476	533	476	482
Proteobacteria (%)			25.75	83.46	83.10	85.64	94.13
	Comamonadaceae	<i>Acidovorax</i>	6.79	53.28	26.67	22.70	7.17
		<i>Hydrogenophaga</i>	0.07	7.73	1.17	2.50	1.01
		<i>Variovorax</i>	0.06	1.46	0.37	0.06	0.03
	Pseudomonadaceae	<i>Pseudomonas</i>	7.63	11.53	26.51	36.63	62.84
		<i>Pseudomonas stutzeri</i>	1.07	1.67	10.17	8.64	4.85
		<i>Pseudomonas lingynensis</i>	6.35	9.56	15.94	27.62	57.08
	Xanthobacteraceae	<i>Ancylobacter</i>	0.14	0.75	14.97	13.84	14.41
	Rhizobiaceae	<i>Rhizobium</i>	0.17	0.80	2.97	1.98	2.94
	Desulfovibrionaceae	<i>Desulfovibrio</i>	0.03	0.07	0.97	0.51	0.39
	Campylobacteraceae	<i>Sulfurospirillum</i>	0.05	0.09	<0.01	<0.01	<0.01
	Geobacteraceae	<i>Geobacter</i>	0.03	<0.01	<0.01	<0.01	<0.01
	Methylophilaceae	<i>Methylophilus</i>	5.52	0.35	1.25	0.64	0.23
Chloroflexi (%)			9.18	11.29	2.55	1.64	2.07
	Dehalococcoidaceae	<i>Dehalococcoides</i>	<0.01	<0.01	<0.01	<0.01	<0.01
Deferribacteres (%)				0.09	1.32	1.13	0.82
	Deferribacteraceae	<i>Denitrovibrio</i>	0.08	1.31	1.12	0.82	0.09
Firmicutes (%)				10.87	0.27	0.16	0.60
	Peptococcaceae	<i>Dehalobacter</i>	<0.01	<0.01	<0.01	<0.01	0.02
		<i>Desulfitobacterium</i>	<0.01	<0.01	<0.01	<0.01	<0.01
		<i>Desulfosporosinus</i>	0.06	0.05	0.27	0.01	0.17
Other (Phyla) (%)			54.10	3.66	13.06	11.30	3.60
		Others (Genera)	79.54	24.95	20.82	11.28	22.78

bioaugmentation with *P. stutzeri* has been successfully used in pilot-scale studies for the remediation of CT-contaminated sites (Penny et al., 2010), the key finding of the natural occurrence of this species and its RA increase by the addition of B<sub>12</sub> makes *P. stutzeri*-mediated remediation strategies promising for the Ödena site.

The *Ancylobacter* genus (classified as *A. dichloromethanicus* or *A. aquaticus*, Table A2) was detected in greater RA (up to 15%, t<sub>3</sub>) in the presence of B<sub>12</sub> than in the absence of B<sub>12</sub> (1%, t<sub>10</sub>) (Table 2), suggesting a correlation with B<sub>12</sub> addition. *A. dichloromethanicus* is an aerobic facultative methylotroph capable of DCM degradation (Firsova et al., 2010). In the CTw/oB treatment, the CF produced was not further degraded to DCM, preventing the proliferation of this species. In contrast, in the 0.01B/CF treatment, the only treatment with significant DCM detection, *Ancylobacter* exhibited 14% RA at t<sub>3</sub> (Table 2), supporting the hypothesis of DCM production and further DCM consumption (pathway 1, Scheme 1). *Ancylobacter* might also be linked to the degradation of structurally closed substrates in the absence of dihalomethanes (Firsova et al., 2010).

As aerobic or facultative-anaerobic bacteria were present in the microcosm, oxygen availability as a co-substrate could be explained by: (i) the occurrence of nitrite-driven processes that would supplement molecular oxygen to monooxygenase activity (Ettwig et al., 2010) as well as to the cometabolism for the degradation of halomethanes; ii) the availability of O<sub>2</sub> from chlorite dismutase activity in *P. stutzeri* (Cladera et al., 2006; Schaffner et al., 2015); iii) in the presence of L-2-haloacid dehalogenases, known to obtain an oxygen atom of the solvent water, in detected species including *A. aquaticus* (Kumar et al., 2016), *P. stutzeri* (Wang et al., 2015), and *Rhizobium sp. RC1* (Adamu et al., 2016) (the last genus with 1–3% RA in all analyzed samples).

### 3.3. Mechanistic insights

CT and CF reduction involves one or two C—Cl bond cleavages in the first rate-limiting step (Elsner et al., 2004; Chan et al., 2012; Lee et al., 2015). For AKIE calculations one C—Cl bond cleavage was assumed and the determined  $\epsilon$  values ( $R^2 \geq 0.9$ ) were used (Table 3, Fig. A8). The AKIE<sub>C</sub> for the 0.01B/CF (1.014 ± 0.002) and for the CTw/oB and 0.01B/CT treatments (1.016 ± 0.003 and 1.013 ± 0.001, respectively) were much below the Streitwieser limit of KIE<sub>C</sub> for complete C—Cl bond cleavage (1.057) (Table A7), and the realistic value of 50% bond cleavage (1.029) (Elsner et al., 2005), making C-Cl cleavage feasible as the rate-limiting step, but showing important masking effects. AKIE<sub>C</sub> was slightly greater in the CTw/oB treatment. The obtained AKIE<sub>C</sub> values are within the range of those obtained for CF microbial reductive dechlorination (1.004–1.028), and below or within the range of those obtained for abiotic CT and CF reductive dechlorination (1.01–1.033 and 1.030–1.034, respectively) (Table A7).

The AKIE<sub>Cl</sub> of the 0.01B/CF treatment (1.0072 ± 0.0004) was lower than the Streitwieser limit for KIE<sub>Cl</sub> (1.013) for a C—Cl bond cleavage, and also lower than the theoretical revised value (1.019) (Paneth, 1992), but it was closer to 50% of the Streitwieser limit (1.0065)

(Elsner et al., 2005), in contrast to the AKIE<sub>C</sub>. Since both elements should be affected by masking to the same extent, this discrepancy suggests chlorine secondary isotopic effects that, in turn, are also masked. Moreover, although there are no AKIE<sub>Cl</sub> values of biotic CF degradation in the literature to compare, the value obtained here was consistent with abiotic CF hydrogenolysis ± the reductive elimination (pathway 1 ± 1a, Scheme 1) by Fe(0) (1.008 ± 0.001) (Torrentó et al., 2017) (Table A7).

For the CTw/oB treatment, the AKIE<sub>Cl</sub> (1.023 ± 0.003) was much above both the theoretical maximum expected KIE<sub>Cl</sub> on a C—Cl bond cleavage (1.013) (Elsner et al., 2005) and the revised value (1.019) (Paneth, 1992). This could be associated with significant secondary isotopic effects (Świderek and Paneth, 2012), with the experimental values exceeding these established theoretical values, as it was also considered for PCE (Badin et al., 2014), or by the cleavage of two C—Cl bonds (KIE = 1.013<sup>2</sup> = 1.026) simultaneously or not to only one C—Cl bond cleavage (Elsner et al., 2004). In contrast, the AKIE<sub>Cl</sub> of CT biodegradation with B<sub>12</sub> (1.015 ± 0.002) was similar to the expected KIE<sub>Cl</sub> values for a C—Cl bond cleavage, probably with a small chlorine secondary isotopic effect or/and only the rare occurrence of two C—Cl bond cleavages, confirming the small differences observed between the CT treatments by AKIE<sub>C</sub>. Thus, mechanistic differences were revealed by the AKIE<sub>Cl</sub> among the CT natural attenuation and B<sub>12</sub> catalyzed reactions. These differences could be related to the fact that the derived AKIE<sub>Cl</sub> of CT is a weighted average of the kinetic effects of different proportions of competing parallel mechanisms in each case (i.e. one vs two C—Cl bond cleavages, leading to ·CCl<sub>3</sub> vs: CCl<sub>2</sub> respectively, Scheme 1), an aspect that is typical from mixed cultures which contain several species capable of pollutant degradation (Nijenhuis and Richnow, 2016). These detected AKIE<sub>Cl</sub> differences between CT natural attenuation and that mediated by B<sub>12</sub> might also be partially uncovering dissimilarities in rate-determining steps preceding C—Cl bond cleavage related to rate limitations in biological reactions (Nijenhuis and Richnow, 2016). In fact, an extracellular catalyst of CT transformation affected by chemical reductants and the presence of transition metals was identified in *P. stutzeri* (Lee et al., 1999; Lewis et al., 2001). Since greater activity of *P. stutzeri* was observed in the presence of B<sub>12</sub>, these extracellular processes might have induced rate-limiting effects, reducing the AKIEs.

### 3.4. Biodegradation pathways discussion

The non-existence or low accumulation of chlorinated by-products such as CF and DCM in all B<sub>12</sub> live treatments, where degradation was confirmed, could highlight two non-excluding hypothesized pathways: 1) the formation of these products and their subsequently rapid consumption following a hydrogenolysis pathway combined or not with the reductive elimination (pathway 1 and 1a, Scheme 1); and/or 2) the reduction of CT or CF ultimately to CO<sub>2</sub> with minor or the inexistent accumulation of CMs (pathway 2, 4). CT thiolytic reduction (pathway 3, Scheme 1) was not confirmed due to the absence of CS<sub>2</sub> accumulation in the main microcosms, although this could also be

**Table 3**  
Carbon and chlorine isotopic fractionation ( $\epsilon_C$  and  $\epsilon_{Cl}$ , respectively) and the corresponding apparent kinetic isotope effect (AKIE<sub>C</sub> and AKIE<sub>Cl</sub>), dual C-Cl isotope slope ( $\Lambda$ ), the dominant metabolically active genus (in relative abundance, RA, %), and the hypothesized pathway for each live treatment. Values from both CT treatments with B<sub>12</sub> were used together for the  $\Lambda$  calculations. t<sub>1</sub>, t<sub>3</sub>, and t<sub>10</sub> represent after 26, 85, and 376 days, respectively. n.m. = not measured since only two data points were available.

Treatment	CFw/oB	0.01B/CF	0.1B/CF	CTw/oB	0.01B/CT	0.1B/CT
$\epsilon_C$ (‰) ± 95% CI	No degradation detected	-14 ± 4	Concentration b.d.l. after t <sub>1</sub>	-16 ± 6	-13 ± 2	n.m.
AKIE <sub>C</sub>		1.014 ± 0.002		1.016 ± 0.001	1.013 ± 0.003	
$\epsilon_{Cl}$ (‰) ± 95% CI		-2.4 ± 0.4		-6 ± 3	-4 ± 2	
AKIE <sub>Cl</sub>		1.0072 ± 0.0004		1.023 ± 0.003	1.015 ± 0.002	
$\Lambda$		7 ± 1		6.1 ± 0.5	5 ± 1	
Dominant genus (RA, %)		<i>Pseudomonas</i> (57), t <sub>3</sub>		<i>Acidovorax</i> (53), t <sub>10</sub>	<i>Acidovorax</i> (27), <i>Pseudomonas</i> (27), t <sub>3</sub>	<i>Pseudomonas</i> (37), t <sub>3</sub>
Hypothesized pathway		Hydrogenolysis ± reductive elimination		Hydrogenolysis among other possible reductions	Different simultaneous reduction processes	

further degraded (Cox et al., 2013). For further pathway conclusions,  $\Delta\delta^{13}\text{C}$  and  $\Delta\delta^{37}\text{Cl}$  of the same treatment and incubation time but measured in different replicates (since similar CT and CF evolution was detected in replicate bottles, Fig. A1) were plotted to obtain the CT and CF  $\Lambda$  values (Fig. 4). For both C and Cl, linear trends ( $R^2 \geq 0.95$ ) were observed. An integrating overview of the different live treatments is shown in Table 3.

The  $\Lambda$  for the 0.01B/CF treatment ( $7 \pm 1$ ) was statistically similar (ANCOVA,  $p = 0.4$ ) to the abiotic CF reduction by Fe(0) ( $8 \pm 2$ ) (Torrentó et al., 2017) (Fig. 4), which supports CF hydrogenolysis  $\pm$  the reductive elimination (pathway 1 and 1a, Scheme 1) as the dominant pathways. CF hydrogenolysis is substantiated by only punctual DCM accumulation after 200 days, and the detection of species capable of DCM dechlorination (e.g. *Ancylobacter dichloromethanicus*). In addition,  $\text{B}_{12}$  might have stimulated CF reductive elimination to CO and  $\text{CO}_2$  as reported previously (Cappelletti et al., 2012). Moreover,  $\Lambda$  was significantly different (ANCOVA,  $p < 0.0001$ ) from the CF abiotic hydrolysis or oxidation ( $13.0 \pm 0.8$ ,  $17 \pm 2$ ) (Torrentó et al., 2017), discarding CF hydrolytic reduction (pathway 2, Scheme 1), assuming the  $\Lambda$  of the reported CF abiotic hydrolysis as a reference system with a C–Cl bond cleavage as a rate-limiting step (Torrentó et al., 2017) and corroborating the absence of oxidation processes.

There was no significant statistical difference between  $\Lambda$  from the 0.01B/CT and 0.1B/CT treatments (Fig. A9) ( $n = 6$ ) (ANCOVA,  $p = 0.23$ ), thus data points from both treatments were plotted together (Fig. 4). The slopes of CT biodegradation with and without  $\text{B}_{12}$  were similar in terms of the 95% CI:  $5 \pm 1$  ( $n = 6$ ) and  $6.1 \pm 0.5$  ( $n = 9$ ), respectively, although ANCOVA analysis showed a significant statistical difference ( $p = 0.02$ ), as evidenced by  $\Lambda$  flattening with the addition of  $\text{B}_{12}$  (Fig. 4). This difference was also suggested by CF accumulation only in the CTw/oB treatment, non-closed isotopic balances, and mechanistic insights results. Metabolically active *P. stutzeri* is capable of readily degrading CT to  $\text{CO}_2$  without CF accumulation (pathway 4, Scheme 1) together with the presence of metabolically active species capable of DCM dechlorination (*Ancylobacter dichloromethanicus*). This supports the coexistence of different reduction pathways when  $\text{B}_{12}$  is present. In order to better understand and quantify the contribution of different CT reaction mechanisms with and without  $\text{B}_{12}$ , further research is extremely needed to obtain  $\Lambda$  representative of CT transformation models.

#### 4. Conclusions

The anaerobic CT natural attenuation potential was confirmed in Òdena site-derived anoxic microcosms, as well as the  $\text{B}_{12}$  catalysing effects on both CT and CF biodegradation. An RNA-based NGS approach showed the metabolically active members (*Acidovorax*, *Pseudomonas*, and *Ancylobacter*) that could be related to the biodegradation of target compounds, that otherwise would be difficult to estimate by means of DNA-based strategies. The dual C–Cl element isotope slope coincidence of CF biodegradation with  $\text{B}_{12}$  and CF abiotic chemical models confirmed the CF hydrogenolysis ( $\pm$  the reductive elimination) pathway, which spurred the use of complementary tools for CF abiotic/biotic hydrogenolysis distinction in future study sites. In addition, the detected differences in CT product distribution,  $\text{AKIE}_{\text{Cl}}$ , and  $\Lambda$  in  $\text{B}_{12}$ -amended and unamended treatments were also consistent with the major relative activity of *P. stutzeri* when  $\text{B}_{12}$  was added, whose natural occurrence is a key finding for effective Òdena remediation. The discretized tracking of by-products was not always conclusive, because some by-products were missed due to further degradation (such as CF or DCM). However, the combination of the isotopic approach and the study of the active indigenous community became of relevant usefulness for evidencing degradation processes. The outcomes of this study create a basis for application of this combined approach in further CMs degradation studies. The 2D-CSIA is a tool to rapidly uncover changes in the field related to the application of CMs remediation strategies, and for pathway identification, although a further thorough assessment of reference  $\Lambda$  which is representative of different CMs reaction mechanisms is necessary. This study is a striking example of the benefits of  $\text{B}_{12}$  in the remediation of complex multi-contaminant polluted sites, which requires a sequential treatment strategy to minimize CF inhibition issues by inducing its transformation. Further feasibility upscaling studies are needed to estimate the required amount of  $\text{B}_{12}$ , to find cheaper  $\text{B}_{12}$  sources, and to elucidate the possible inhibition effects of  $\text{B}_{12}$ -related intermediates (phosgene, thiophosgene) on the degradation of CMs. Furthermore, since the co-deposition of nitrate and VOCs is widespread in soils and groundwater worldwide (Squillace et al., 2002), the presence of metabolically active denitrifying genera (*Pseudomonas*, *Rhizobium*, or *Acidovorax*) which are linked to CT and CF biodegradation in the present experiments, raises interest in the study of the co-metabolism of both pollutants as a potential bioremediation strategy.

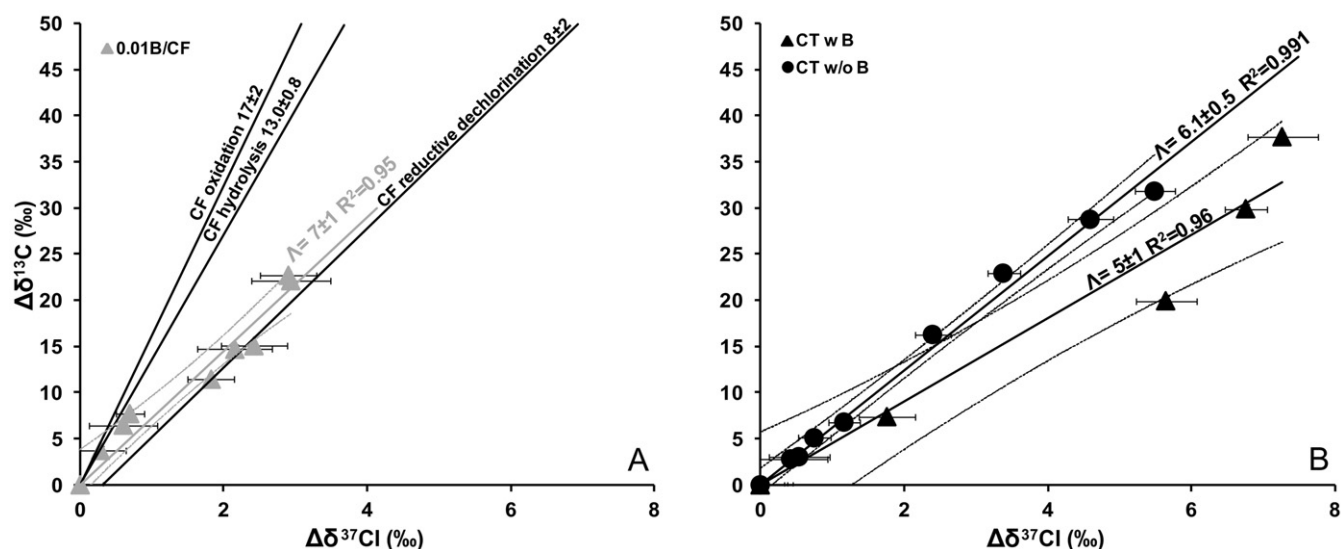


**Fig. 4.** Dual C–Cl isotope plot for CF (A) and CT (B) biodegradation data observed in the microcosms. Solid grey in A and black lines in B correspond to linear regressions of the data sets obtained in this study with 95% CI (dashed lines). Error bars show uncertainty in duplicate isotope measurements. Note that the error bars of the  $\Delta\delta^{13}\text{C}$  values are smaller than the symbols. The CF oxidation by thermally-activated persulphate, CF alkaline hydrolysis, and CF reductive dechlorination by Fe(0) slopes in A (black lines) correspond to the CF abiotic degradation reference systems (Torrentó et al., 2017).

## Author contributions

The manuscript was written through contributions of all authors. All authors have given approval to the final version of the manuscript.

## Acknowledgements

This research was supported by a Marie Curie Career Integration Grant in the framework of IMOTEC-BOX project (PCIG9-GA-2011-293808), the Spanish Government ATTENUATION (CGL2011-29975-C04-01) and REMEDIATION (CGL2014-57215-C4-1-R) projects and the Catalan Government project 2014SGR-1456. We thank technical support from CCIT-UB and Dr. J. Vila. D. Rodríguez-Fernández acknowledges FPU2012/01615 and Beca Fundació Pedro i Pons 2014 and M. Rosell, Ramón y Cajal contract (RYC-2012-11920). We thank the editor and two anonymous reviewers for comments that improved the quality of the manuscript.

## Appendix A. Supplementary data

Supplementary data to this article can be found online at <https://doi.org/10.1016/j.scitotenv.2017.10.067>.

## References

- Adamu, A., Wahab, R.A., Huyop, F., 2016. L-2-Haloacid dehalogenase (DehL) from *Rhizobium* sp. RC1. *Spring 5*, 695. <https://doi.org/10.1186/s40064-016-2328-9>.
- Adrian, L., Löffler, E.F. (Eds.), 2016. *Organohalide-respiring Bacteria*. Springer, Berlin Heidelberg <https://doi.org/10.1007/978-3-662-49875-0>.
- Badin, A., Buttet, G., Maillard, J., Holliger, C., Hunkeler, D., 2014. Multiple dual C-Cl isotope patterns associated with reductive dechlorination of tetrachloroethene. *Environ. Sci. Technol.* 48:9179–9186. <https://doi.org/10.1021/es500822d>.
- Bagley, D.M., Lalonde, M., Kaseros, V., Stasiuk, K.E., Sleep, B.E., 2000. Acclimation of anaerobic systems to biodegrade tetrachloroethene in the presence of carbon tetrachloride and chloroform. *Water Res.* 34:171–178. [https://doi.org/10.1016/S0043-1354\(99\)00121-9](https://doi.org/10.1016/S0043-1354(99)00121-9).
- Banerjee, R., Ragsdale, S.W., 2003. The many faces of vitamin B<sub>12</sub>: catalysis by cobalamin-dependent enzymes. *Annu. Rev. Biochem.* 72:209–247. <https://doi.org/10.1146/annurev.biochem.72.121801.161828>.
- Becker, J.G., Freedman, D.L., 1994. Use of cyanocobalamin to enhance anaerobic biodegradation of chloroform. *Environ. Sci. Technol.* 28:1942–1949. <https://doi.org/10.1021/es00060a027>.
- Caporaso, J., Bittinger, K., Bushman, F.D., Desantis, T.Z., Andersen, G.L., Knight, R., 2010a. PyNAST: a flexible tool for aligning sequences to a template alignment. *Bioinformatics* 26:266–267. <https://doi.org/10.1093/bioinformatics/btp636>.
- Caporaso, J., Kuczynski, J., Stombaugh, J., Bittinger, K., Bushman, F.D., Costello, E.K., Fierer, N., Peña, A.G., Goodrich, J.K., Gordon, J.L., Huttley, G.A., Kelley, S.T., Knights, D., Koenig, J.E., Ley, R.E., Lozupone, C.A., McDonald, D., Muegge, B.D., Pirrung, M., Reeder, J., Sevinsky, J.R., Turnbaugh, P.J., Walters, W.A., Widmann, J., Yatsunenko, T., Zaneveld, J., Knight, R., 2010b. QIIME allows analysis of high-throughput community sequencing data intensity normalization improves color calling in SOLiD sequencing. *Nat. Publ. Gr.* 7:335–336. <https://doi.org/10.1038/nmeth0510-335>.
- Cappelletti, M., Frascari, D., Zannoni, D., Fedi, S., 2012. Microbial degradation of chloroform. *Appl. Microbiol. Biotechnol.* 96:1395–1409. <https://doi.org/10.1007/s00253-012-4494-1>.
- Chakraborty, A., Roden, E.E., Schieber, J., Picardal, F., 2011. Enhanced growth of *Acidovorax* sp. strain 2AN during nitrate-dependent Fe(II) oxidation in batch and continuous-flow systems. *Appl. Environ. Microbiol.* 77:8548–8556. <https://doi.org/10.1128/AEM.06214-11>.
- Chan, C.C.H., Mundle, S.O.C., Eckert, T., Liang, X., Tang, S., Lacrampe-Couloume, G., Edwards, E.A., Sherwood Lollar, B., 2012. Large carbon isotope fractionation during biodegradation of chloroform by *Dehalobacter* cultures. *Environ. Sci. Technol.* 46:10154–10160. <https://doi.org/10.1021/es3010317>.
- Cladera, A.M., García-Valdés, E., Lalucat, J., 2006. Genotype versus phenotype in the circumscription of bacterial species: the case of *Pseudomonas stutzeri* and *Pseudomonas chloritidis* mutants. *Arch. Microbiol.* 184:353–361. <https://doi.org/10.1007/s00203-005-0052-x>.
- Cox, S.F., McKinley, J.D., Ferguson, A.S., O'Sullivan, G., Kalin, R.M., 2013. Degradation of carbon disulphide (CS<sub>2</sub>) in soils and groundwater from a CS<sub>2</sub>-contaminated site. *Environ. Earth Sci.* 68:1935–1944. <https://doi.org/10.1007/s12665-012-1881-y>.
- Cretnik, S., Thoreson, K.A., Bernstein, A., Ebert, K., Buchner, D., Laskov, C., Haderlein, S., Shoukar-Stash, O., Kliegman, S., McNeill, K., Elsner, M., 2013. Reductive dechlorination of TCE by chemical model systems in comparison to dehalogenating bacteria: insights from dual element isotope analysis (<sup>13</sup>C/<sup>12</sup>C, <sup>37</sup>Cl/<sup>35</sup>Cl). *Environ. Sci. Technol.* 47:6855–6863. <https://doi.org/10.1021/es400107n>.
- Desantis, T.Z., Hugenholtz, P., Larsen, N., Rojas, M., Brodie, E.L., Keller, K., Huber, T., Dalevi, D., Hu, P., Andersen, G.L., 2006. Greengenes, a chimera-checked 16S rRNA gene database and workbench compatible with ARB. *Appl. Environ. Microbiol.* 72:5069–5072. <https://doi.org/10.1128/AEM.03006-05>.
- Ding, C., Zhao, S., He, J., 2014. A *Desulfotobacterium* sp. strain PR reductively dechlorinates both 1,1,1-trichloroethane and chloroform. *Environ. Microbiol.* 16:3387–3397. <https://doi.org/10.1111/1462-2920.12387>.
- Doherty, R., 2000. A history of the production and use of carbon tetrachloride, tetrachloroethylene, trichloroethylene and 1,1,1-trichloroethane in the United States: part 1 – historical background; carbon tetrachloride and tetrachloroethylene. *Environ. Forensics* 1, 175.
- Duhamel, M., Wehr, S.D., Yu, L., Rizvi, H., Seepersad, D., Dworatzek, S., Cox, E.E., Edwards, E.A., 2002. Comparison of anaerobic dechlorinating enrichment cultures maintained on tetrachloroethene, trichloroethene, cis-dichloroethene and vinyl chloride. *Water Res.* 36:4193–4202. [https://doi.org/10.1016/S0043-1354\(02\)00151-3](https://doi.org/10.1016/S0043-1354(02)00151-3).
- Edgar, R.C., 2010. Search and clustering orders of magnitude faster than BLAST. *Bioinformatics* 26:2460–2461. <https://doi.org/10.1093/bioinformatics/btq461>.
- Egli, C., Stromeyer, S., Cook, A.M., Leisinger, T., 1990. Transformation of tetra- and trichloromethane to CO<sub>2</sub> by anaerobic bacteria is a non-enzymic process. *FEMS Microbiol. Lett.* 68, 207–212.
- Elsner, M., 2010. Stable isotope fractionation to investigate natural transformation mechanisms of organic contaminants: principles, prospects and limitations. *J. Environ. Monit.* 12:2005–2031. <https://doi.org/10.1039/c0em00277a>.
- Elsner, M., Haderlein, S.B., Kellerhals, T., Luzzi, S., Zwank, L., Angst, W., Schwarzenbach, R.P., 2004. Mechanisms and products of surface-mediated reductive dehalogenation of carbon tetrachloride by Fe(II) on goethite. *Environ. Sci. Technol.* 38:2058–2066. <https://doi.org/10.1021/es034741m>.
- Elsner, M., Zwank, L., Hunkeler, D., Schwarzenbach, R.P., 2005. A new concept linking observable stable isotope fractionation to transformation pathways of organic pollutants. *Environ. Sci. Technol.* 39, 6896–6916.
- Ettwig, K.F., Butler, M.K., Le Paslier, D., Pelletier, E., Mangenot, S., Kuypers, M.M.M., Schreiber, F., Dutilh, B.E., Zedelius, J., de Beer, D., et al., 2010. Nitrite-driven anaerobic methane oxidation by oxygenic bacteria. *Nature* 464:543–548. <https://doi.org/10.1038/nature08883>.
- Fennell, D.E., Carroll, A.B., Gossett, J.M., Zinder, S.H., 2001. Assessment of indigenous reductive dechlorinating potential at a TCE-contaminated site using microcosms, polymerase chain reaction analysis, and site data. *Environ. Sci. Technol.* 35:1830–1839. <https://doi.org/10.1021/es0016203>.
- Field, J.A., Sierra-Alvarez, R., 2004. Biodegradability of chlorinated solvents and related chlorinated aliphatic compounds. *Rev. Environ. Sci. Biotechnol.* 3:185–254. <https://doi.org/10.1007/s11157-004-4733-8>.
- Firsova, J.E., Doronina, N.V., Trotsenko, Y.A., 2010. Analysis of the key functional genes in new aerobic degraders of dichloromethane. *Mikrobiologiya* 79:72–78. <https://doi.org/10.1134/S0026261710010091>.
- Futagami, T., Yamaguchi, T., Nakayama, S.I., Goto, M., Furukawa, K., 2006. Effects of chloromethanes on growth of and deletion of the *pce* gene cluster in dehalorespiring *Desulfotobacterium hafniense* strain Y51. *Appl. Environ. Microbiol.* 72:5998–6003. <https://doi.org/10.1128/AEM.00979-06>.
- Guerrero-Barajas, C., Field, J.A., 2005a. Riboflavin- and cobalamin-mediated biodegradation of chloroform in a methanogenic consortium. *Biotechnol. Bioeng.* 89:539–550. <https://doi.org/10.1002/bit.20379>.
- Guerrero-Barajas, C., Field, J.A., 2005b. Enhancement of anaerobic carbon tetrachloride biotransformation in methanogenic sludge with redox active vitamins. *Biodegradation* 16:215–228. <https://doi.org/10.1007/s10532-004-0638-z>.
- Haas, B.J., Gevers, D., Earl, A.M., Feldgarden, M., Ward, D.V., Giannoukos, G., Ciulla, D., Tabbaa, D., Highlander, S.K., Sodergren, E., Methé, B., Desantis, T.Z., The Human Microbiome Consortium, Petrosino, J.F., Knight, R., Birren, B.W., 2011. Chimeric 16S rRNA sequence formation and detection in Sanger and 454-Pyrosequenced PCR amplicons. *Genome Res.* 21:494–504. <https://doi.org/10.1101/gr.112730.110.Freely>.
- Hashsham, S.A., Scholze, R., Freedman, D.L., 1995. Cobalamin-enhanced anaerobic biotransformation of carbon tetrachloride. *Environ. Sci. Technol.* 29, 2856–2863.
- He, Y.T., Wilson, J.T., Su, C., Wilkin, R.T., 2015. Review of abiotic degradation of chlorinated solvents by reactive iron minerals in aquifers. *Groundw. Monit. Remediat.* 35:57–75. <https://doi.org/10.1111/gwmr.12111>.
- Heckel, B., Rodríguez-Fernández, D., Torrentó, D., Meyer, A., Palau, J., Domènech, C., Rosell, M., Soler, A., Hunkeler, D., Elsner, D., 2017. Compound-specific chlorine isotope analysis of tetrachloromethane and trichloromethane by GC-IRMS vs. GC-qMS: method development and evaluation of precision and trueness. *Anal. Chem.* 89:3411–3420. <https://doi.org/10.1021/acs.analchem.6b04129>.
- International Agency for Research on Cancer, 2016. IARC Monographs on the Evaluation of Carcinogenic Risks to Humans. [WWW Document]. [http://monographs.iarc.fr/ENG/Classification/latest\\_classif.php](http://monographs.iarc.fr/ENG/Classification/latest_classif.php) (accessed 5.24.16).
- Kumar, A., Pillay, B., Olaniran, A.O., 2016. L-2-Haloacid dehalogenase from *Ancylobacter aquaticus* UV5: sequence determination and structure prediction. *Int. J. Biol. Macromol.* 83:216–225. <https://doi.org/10.1016/j.ijbiomac.2015.11.066>.
- Lee, C.H., Lewis, T.A., Paszczynski, A., Crawford, R.L., 1999. Identification of an extracellular catalyst of carbon tetrachloride dehalogenation from *Pseudomonas stutzeri* strain KC as pyridine-2, 6-bis(thiocarboxylate). *Biochem. Biophys. Res. Commun.* 261:562–566. <https://doi.org/10.1006/bbrc.1999.1077>.
- Lee, M., Wells, E., Wong, Y.K., Koenig, J., Adrian, L., Richnow, H.H., Manefield, M., 2015. Relative contributions of *Dehalobacter* and zerovalent iron in the degradation of chlorinated methanes. *Environ. Sci. Technol.* 49:4481–4489. <https://doi.org/10.1021/es5052364>.
- Lewis, T.A., Crawford, R.L., 1995. Transformation of carbon tetrachloride via sulfur and oxygen substitution by *Pseudomonas* sp. strain KC. *J. Bacteriol.* 177, 2204–2208.
- Lewis, T.A., Paszczynski, A., Gordon-Wylie, S.W., Jeedigunta, S., Lee, C.H., Crawford, R.L., 2001. Carbon tetrachloride dechlorination by the bacterial transition metal chelator

- pyridine-2,6-bis(thiocarboxylic acid). *Environ. Sci. Technol.* 35:552–559. <https://doi.org/10.1021/es001419s>.
- Lima, G. da P., Sleep, B.E., 2010. The impact of carbon tetrachloride on an anaerobic methanol-degrading microbial community. *Water Air Soil Pollut.* 212:357–368. <https://doi.org/10.1007/s11270-010-0350-z>.
- Martín-González, L., Mortan, S.H., Rosell, M., Parladé, E., Martínez-Alonso, M., Gaju, N., Caminal, G., Adrian, L., Marco-Urrea, E., 2015. Stable carbon isotope fractionation during 1,2-dichloropropane-to-propene transformation by an enrichment culture containing *Dehalogenimonas* strains and a *dcpA* gene. *Environ. Sci. Technol.* 49:8666–8674. <https://doi.org/10.1021/acs.est.5b00929>.
- Nijenhuis, I., Richnow, H.H., 2016. Stable isotope fractionation concepts for characterizing biotransformation of organohalides. *Curr. Opin. Biotechnol.* 41:108–113. <https://doi.org/10.1016/j.copbio.2016.06.002>.
- Palatsi, J., Illa, J., Prenafeta-Boldú, F.X., Lauren, M., Fernandez, B., Angelidaki, I., Flotats, X., 2010. Long-chain fatty acids inhibition and adaptation process in anaerobic thermophilic digestion: batch tests, microbial community structure and mathematical modelling. *Bioresour. Technol.* 101:2243–2251. <https://doi.org/10.1016/j.biortech.2009.11.069>.
- Palau, J., Marchesi, M., Chambon, J.C.C., Aravena, R., Canals, À., Binning, P.J., Bjerg, P.L., Otero, N., Soler, A., 2014. Multi-isotope (carbon and chlorine) analysis for fingerprinting and site characterization at a fractured bedrock aquifer contaminated by chlorinated ethenes. *Sci. Total Environ.* 475:61–70. <https://doi.org/10.1016/j.scitotenv.2013.12.059>.
- Paneth, P., 1992. How to measure heavy atom isotope effects: general principles. In: Bunzel, E., Saunders, W.H.J. (Eds.), *Isotopes in Organic Chemistry*. Elsevier, New York, p. 192.
- Pelissari, C., Guivernau, M., Viñas, M., de Souza, S.S., García, J., Sezerino, P.H., Ávila, C., 2017. Unraveling the active microbial populations involved in nitrogen utilization in a vertical subsurface flow constructed wetland treating urban wastewater. *Sci. Total Environ.* 584–585:642–650. <https://doi.org/10.1016/j.scitotenv.2017.01.091>.
- Penny, C., Vuilleumier, S., Bringel, F., 2010. Microbial degradation of tetrachloromethane: mechanisms and perspectives for bioremediation. *FEMS Microbiol. Ecol.* 74:257–275. <https://doi.org/10.1111/j.1574-6941.2010.00935.x>.
- Puigserver, D., Nieto, J.M., Grifoll, M., Vila, J., Cortés, A., Viladevall, M., Parker, B.L., Carmona, J.M., 2016. Temporal hydrochemical and microbial variations in microcosm experiments from sites contaminated with chloromethanes under biostimulation with lactic acid. *Bioremediat. J.* 20:54–70. <https://doi.org/10.1080/10889868.2015.1124061>.
- Reeder, J., Knight, R., 2010. Rapidly denoising pyrosequencing amplicon reads by exploiting rank-abundance distributions. *Nat. Methods* 7:668–669. <https://doi.org/10.1038/nmeth0910-668b>.
- Riley, R.G., Szecsody, J.E., Sklarew, D.S., Mitroshkov, A.V., Gent, P.M., Brown, C.F., Thompson, C.J., 2010. Desorption behaviour of carbon tetrachloride and chloroform in contaminated low organic carbon aquifer sediments. *Chemosphere* 79:807–813. <https://doi.org/10.1016/j.chemosphere.2010.03.005>.
- Schaffner, I., Hofbauer, S., Krutzler, M., Pirker, K.F., Furtmüller, P.G., Obinger, C., 2015. Mechanism of chlorite degradation to chloride and dioxygen by the enzyme chlorite dismutase. *Arch. Biochem. Biophys.* 574:18–26. <https://doi.org/10.1016/j.abb.2015.02.031>.
- Schloss, P.D., Westcott, S.L., Ryabin, T., Hall, J.R., Hartmann, M., Hollister, E.B., Lesniewski, R.A., Oakley, B.B., Parks, D.H., Robinson, C.J., Sahl, J.W., Stres, B., Thallinger, G.G., Van Horn, D.J., Weber, C.F., 2009. Introducing mothur: open-source, platform-independent, community-supported software for describing and comparing microbial communities. *Appl. Environ. Microbiol.* 75:7537–7541. <https://doi.org/10.1128/AEM.01541-09>.
- Shan, H., Kurtz, H.D., Freedman, D.L., 2010. Evaluation of strategies for anaerobic bioremediation of high concentrations of halomethanes. *Water Res.* 44:1317–1328. <https://doi.org/10.1016/j.watres.2009.10.035>.
- Sherdwood Lollar, B., Hirschorn, S.K., Chartrand, M.M.G., Lacrampe-Couloume, G., 2007. An approach for assessing total instrumental uncertainty in compound-specific isotope analysis: implications for environmental remediation studies. *Anal. Chem.* 79:3469–3475. <https://doi.org/10.1021/ac062299v>.
- Song, H., Carraway, E.R., 2006. Reduction of chlorinated methanes by nano-sized zero-valent iron. Kinetics, pathways and effect of reaction conditions. *Environ. Eng. Sci.* 23, 272–284.
- Squillace, P.J., Scott, J.C., Moran, M.J., Nolan, B.T., Kolpin, D.W., 2002. VOCs, pesticides, nitrate, and their mixtures in groundwater used for drinking water in the United States. *Environ. Sci. Technol.* 36:1923–1930. <https://doi.org/10.1021/es015591n>.
- Staudinger, J., Roberts, P.V., 2001. A critical compilation of Henry's law constant temperature dependence relations for organic compounds in dilute aqueous solutions. *Chemosphere* 44:561–576. [https://doi.org/10.1016/S0045-6535\(00\)00505-1](https://doi.org/10.1016/S0045-6535(00)00505-1).
- Świderek, K., Paneth, P., 2012. Extending limits of chlorine kinetic isotope effects. *J. Organomet. Chem.* 77:5120–5124. <https://doi.org/10.1021/jo300682f>.
- Tang, S., Edwards, E.A., 2013. Identification of *Dehalobacter* reductive dehalogenases that catalyze dechlorination of chloroform, 1,1,1-trichloroethane and 1,1-dichloroethane. *Philos. Trans. R. Soc. B* 368, 20120318. <https://doi.org/10.1098/rstb.2012.0318>.
- Tang, S., Wang, P.H., Higgins, S.A., Löffler, F.E., Edwards, E.A., 2016. Sister *Dehalobacter* genomes reveal specialization in organohalide respiration and recent strain differentiation likely driven by chlorinated substrates. *Front. Microbiol.* 7:1–14. <https://doi.org/10.3389/fmicb.2016.00100>.
- Torrentó, C., Audí-Miró, C., Bordeleau, G., Marchesi, M., Rosell, M., Otero, N., Soler, A., 2014. The use of alkaline hydrolysis as a novel strategy for chloroform remediation: the feasibility of using construction wastes and evaluation of carbon isotopic fractionation. *Environ. Sci. Technol.* 48:1869–1877. <https://doi.org/10.1021/es403838t>.
- Torrentó, C., Palau, J., Rodríguez-Fernández, D., Heckel, B., Meyer, A., Domènech, C., Rosell, M., Soler, A., Elsner, M., Hunkeler, D., 2017. Carbon and chlorine isotope fractionation patterns associated with different engineered chloroform transformation reactions. *Environ. Sci. Technol.* 51:6174–6184. <https://doi.org/10.1021/acs.est.7b00679>.
- Wang, Q., Garrity, G.M., Tiedje, J.M., Cole, J.R., 2007. Naive Bayesian classifier for rapid assignment of rRNA sequences into the new bacterial taxonomy. *Appl. Environ. Microbiol.* 73 (16), 5261–5267.
- Wang, Y., Xin, Y., Cao, X., Xue, S., 2015. Enhancement of L-2-haloacid dehalogenase expression in *Pseudomonas stutzeri* DEH138 based on the different substrate specificity between dehalogenase-producing bacteria and their dehalogenases. *World J. Microbiol. Biotechnol.* 31:669–673. <https://doi.org/10.1007/s11274-015-1817-2>.
- Workman, D.J., Woods, S.L., Gorby, Y.A., Fredrickson, J.K., Truex, M.J., 1997. Microbial reduction of vitamin B12 by *Shewanella alga* strain BrY with subsequent transformation of carbon tetrachloride. *Environ. Sci. Technol.* 31:2292–2297. <https://doi.org/10.1021/es960880a>.
- Yargicoglu, E.N., Reddy, K.R., 2015. Review of biological diagnostic tools and their applications in geoenvironmental engineering. *Rev. Environ. Sci. Biotechnol.* 14:161–194. <https://doi.org/10.1007/s11157-014-9358-y>.
- Zou, S., Stensel, H.D., Ferguson, J.F., 2000. Carbon tetrachloride degradation: effect of microbial growth substrate and vitamin B<sub>12</sub> content. *Environ. Sci. Technol.* 34:1751–1757. <https://doi.org/10.1021/es990930m>.
- Zwank, L., Elsner, M., Aeberhard, A., Schwarzenbach, R.P., 2005. Carbon isotope fractionation in the reductive dehalogenation of carbon tetrachloride at iron (hydr)oxide and iron sulfide minerals. *Environ. Sci. Technol.* 39, 5634–5641.